Manipulation and characterisation of accumulation and coarse mode aerosol particles using a Bessel beam trap

Helena Meresman,[a] Jon B. Wills,[a] Michael Summers,[b] David McGloin[c] and Jonathan P. Reid*[a]

Received 15th July 2009, Accepted 16th September 2009
First published as an Advance Article on the web 5th November 2009
DOI: 10.1039/b914165k

Micron and sub-micron sized aerosol particles are captured, manipulated and characterised in a Bessel beam optical trap. Bright field microscopy and elastic light scattering measurements are used in combination to interrogate trapped particles and explore the optical landscape of the trap. We conclude that the Bessel trap has a number of advantages over optical tweezers in terms of characterisation of accumulation mode particles, manipulation of particles over macroscopic length scales and effective control of the gas phase. As such, the Bessel trap is a valuable addition to the aerosol optical toolkit.

I. Introduction

An ability to sample and trap aerosol particles in the accumulation and coarse size modes and to manipulate them on the macro-scale is an important goal for experimentalists concerned with developing new technologies to probe atmospheric, industrial and therapeutic aerosols. Aerosol media display unique properties that can have considerable bearing on their environment. For example, aerosols in the atmosphere have a significant effect on fundamental climate properties such as air quality and temperature.[1,2] The sampling and characterisation of aerosols presents a number of technical challenges to which optical techniques can offer an effective solution. Ensemble field measurements of aerosols *in situ* are routinely carried out using optical absorption and scattering spectroscopies. Although fast and accurate, ensemble measurements yield average values for parameters such as composition and size. From such information it is often impossible to extract the precise mixing state and phase characteristics of the component particles, key characteristics that determine the properties of the ensemble. In addition, single particle studies using electrostatic and optical trapping tools are necessary to thoroughly explore aerosol properties.

This paper is devoted to establishing the potential of an optical manipulation technique which utilises a pseudo-non-diffracting Bessel laser beam in combination with other optical characterisation methods as a powerful multi-functional analytical tool for capturing individual aerosol particles and probing their properties. One particular advantage of incorporating a Bessel beam into *in situ* aerosol analysis is rooted in its guiding capabilities. The vertical guiding distance of liquid aerosol droplets in air has been shown to be up to 2.8 mm, depending on the composition and refractive index of the aerosol.[3] This provides considerable flexibility in the trapping position and enables the particle to be probed in an unperturbed environment some distance away from any optical components or surfaces. Further, when the cross-section and the axial extent of the Bessel trap are considered, the sampling volume within which aerosol can be captured is considerably larger than more conventional optical and electrostatic traps. Combining the long guiding distance ability of Bessel traps with the capability to probe the size, composition, morphology, refractive index and spatial dynamics of aerosols, which can be achieved by various spectroscopic techniques, could allow accurate *in situ* measurements of fundamental aerosol properties.

The main property that influences the guiding distance of a Bessel beam is the resistance of the beam to diffraction. Even a collimated, low divergence laser beam is still subject to diffraction, which causes it to spread. The typical parameter used to define the divergence of a Gaussian beam is the Rayleigh range, Z_r, which describes the distance over which the cross-section of the beam increases by a factor of two and can be estimated from the beam waist at focus, w_0,

$$Z_r = \frac{\pi w_0^2}{\lambda} \quad (1)$$

where λ is the wavelength of the light. For a Gaussian beam with beam waist of 5 μm, the Rayleigh range is just 0.15 mm. This diffractive spreading makes guiding using Gaussian beams inefficient due to the increasing power requirements as the particle moves away from the beam waist minimum. If the diffraction of the beam can be avoided, long distance lower power particle guiding becomes achievable and particles can be manipulated and interrogated far from any optical components which may perturb the gas phase surrounding the particle. The distance over which the diameter of the central core of the Bessel beam remains unchanged is much larger than that of a Gaussian beam and, thus, the spatial constraint on the axial position of the trapped particle along the beam propagation direction is reduced. Indeed, the guiding distance achieved with a Bessel beam has been shown to be as much as

[a] *School of Chemistry, University of Bristol, Bristol, UK BS8 1TS. E-mail: j.p.reid@bristol.ac.uk*
[b] *Physical and Theoretical Chemistry, University of Oxford, Oxford, UK OX1 3PN*
[c] *SUPA, Electronic Engineering and Physics Division, University of Dundee, Dundee, UK DD1 4HN*

a factor of ten larger than is achieved with a Gaussian beam of comparable beam waist at beam focus. In addition, greater lateral confinement of particles is achievable along the length of the guiding region, perpendicular to the axis of beam propagation,[3] as the beam core-width is not diffraction limited.

Bessel light beams are characterised by a bright non-diffracting central core with a diameter as little as $\frac{3}{4}$ of the beam wavelength. The transverse intensity profile of a zeroth order Bessel beam exhibits the periodic properties of a set of evenly distributed concentric rings with the total integrated power carried by each ring approximately equal to that of the central core.[3,4] The core does not diverge significantly over the propagation distance of the beam, Z_{max}, and is capable of self-reconstruction upon meeting with an obstacle. Theoretically, a Bessel beam consists of an infinite number of rings carrying infinite energy over an infinite distance. Such a beam is experimentally unrealisable, but Durnin *et al.* demonstrated that an approximation to the ideal zero order Bessel beam can indeed be achieved in the laboratory.[5] Such a quasi-Bessel beam preserves the important properties of the ideal Bessel beam, such as resistance to diffractive spreading and transverse intensity profile.

In the measurements described here, an axicon is used to create the Bessel beam, which generates a set of light waves propagating on a cone, with the cone angle given by:

$$\vartheta = (n - 1)\gamma, \tag{2}$$

where n is the refractive index of the axicon and γ is its opening angle. The propagation distance of the non-diffracting region is given by:

$$Z_{max} = \frac{w}{(n-1)\gamma}, \tag{3}$$

where w is the diameter of the incident Gaussian beam.

We demonstrate that the size of aerosol particles captured within a Bessel beam can be characterised by light scattering techniques. More specifically, the phase function is recorded in the horizontal plane at a scattering angle of 90° to the propagation direction of an incident laser beam at 632.8 nm. To our knowledge, this represents the first ever demonstration that particles held within a Bessel beam, either within a liquid or gaseous medium, can be characterised by conventional techniques. We demonstrate that the guiding distance of aerosol particles is independent of size and that sub-micron sized particles can be controlled and characterised in a Bessel beam. Finally, we compare this approach for sampling and manipulating aerosol particles to a single-beam gradient force optical trap (optical tweezers).

II. Experimental description

A schematic diagram of the experimental apparatus is shown in Fig. 1. A single Bessel beam propagating along the vertical axis was created with a Gaussian 532 nm Nd:YVO4 laser (Coherent VERDI V5). The Bessel beam is generated with an axicon with an opening angle of 3° and a double telescope lens arrangement. The beam is first passed through a collimator to expand the beam diameter illuminating the axicon. The beam

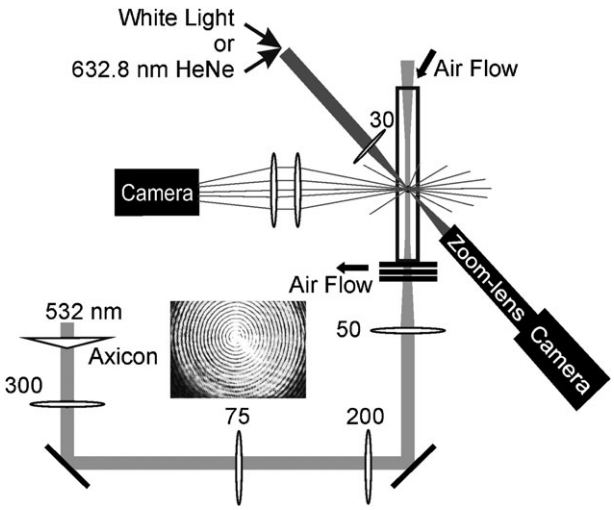

Fig. 1 Schematic representation of the experimental set-up. The focal lengths of the lenses used are shown in mm. The transverse cross-section of the Bessel beam is also shown (inset).

then passes through the double telescope in order to optimise its propagation distance and core size. This results in a Bessel beam with 15 rings, a central core diameter of 5 μm, and a propagation distance of approximately 1.5 mm, determined by imaging of the axial and longitudinal beam profile. The transverse beam profile is shown inset in Fig. 1. The experimental cell used here is not sealed from surrounding air circulation and it is necessary to stabilise the trapped droplet by introducing a downward force in the form of a constant air flow using an air pump (Ametek MICROjammer). By increasing the downward drag on the particle and the levitating Bessel beam power, the trap becomes more robust against surrounding air perturbations. The lower limit on the trapping power used is set at a total laser power of around 250 mW, corresponding to ~17 mW in the core. Using this set-up, we were able to levitate a droplet for as long as 40 min or more. By comparison typical trapping powers for the levitation of liquid droplets in stagnant air may be as low as 1 mW.[6] This lower value reflects the absence of a downward drag force and also reduced air turbulence due to a closed cell arrangement.

To record the phase function, the trapped droplet is illuminated with light from a horizontally polarised HeNe laser (Melles Griot, 5 mW maximum output, 632.8 nm wavelength), which is loosely focused with 30 mm focal distance lens. Scattered light is collected at 90° to the incident HeNe beam with a 50 mm diameter, 50 mm focal length lens positioned approximately 59 mm away from the droplet giving a collection angle of 46.2°. The choice of the larger diameter lens for collection allows a larger segment of the wavefront to be recorded. A further lens (25 mm focal length) is used to image the scatter onto a CCD camera. Two filters are used to reduce the contribution of the elastic scatter from the trapping Nd:YVO4 laser, a 532 nm laser mirror (Laseroptik) and a 532 nm notch filter (Semrock, StopLine).

To acquire a bright field image of a droplet, a zoom lens (Navitar, Zoom 6000) is positioned at 90° to the vertical axis of the Bessel beam, in the horizontal plane. The zoom lens

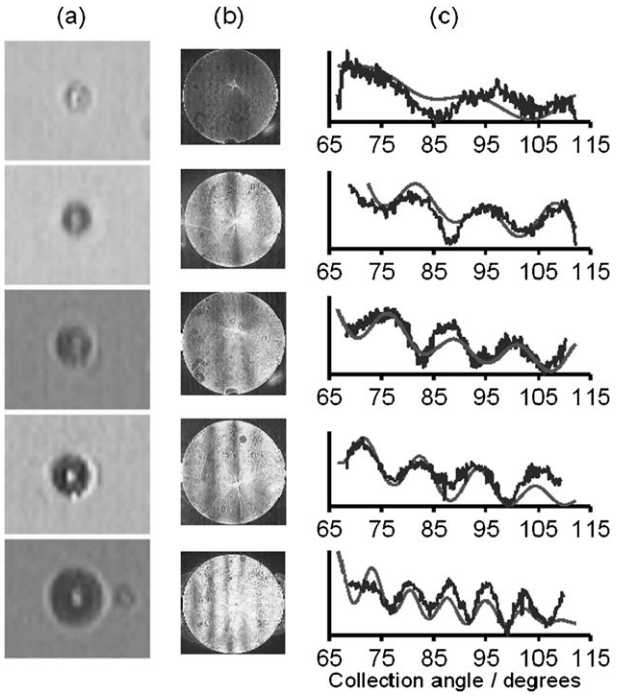

Fig. 2 (a) Bright field images, (b) scattering images and (c) associated phase functions for five droplets trapped in the Bessel beam. The smooth curves overlaying the phase plots are best fits to Mie scattering calculations, the fitted droplet diameters are (from top to bottom): 1.7; 2.5; 2.6; 3.1 and 4.5 μm.

system involves an objective (Mitoyu, 20× magnification, infinity corrected, NA of 0.42) with a long working distance coupled to a zoom lens (6.5–1.0 ratio) and a 1× adapter. The overall magnification of the system is up to 45.72× and the working distance is 25 to 35 mm. A CCD camera is used to collect the image. Again, coloured glass filters are placed in front of the camera to reduce green scatter. Illumination is provided by a white light source introduced through a fibre bundle. The experimental geometry prevents simultaneous illumination of a droplet with both HeNe laser and white light and collection of phase functions and images. Therefore the recordings of phase function and bright field image must be alternated, with a time difference between the measurements of approximately 15 s.

Aerosol droplets are generated with a medical nebuliser (Schill Medical aerosonic travel, mean measured aerosol radius *ca.* 3.5 μm) from an aqueous solution containing 80 g L^{-1} sodium chloride. The flow of droplets is introduced to the experimental cell from the top. Gravity, along with the downward air flow, draws the droplets through the Bessel beam, and some become trapped therein. To protect the optical elements, a coverslip is placed at the bottom of the cell above the last lens and just below the air flow exit. The excess droplets are either collected on the coverslip or on a filter prior to the air pump. The experimental cell is fabricated from a square-section optical glass tube, with polished windows on all four sides and with a 100 mm longitudinal pathway along the propagation direction of the laser beam. The trapping region of the beam is positioned approximately 2 cm above the coverslip, consistent with our previous discussion that the trap can be established remote from optical components.

III. Droplet size determination

The radiation pressure required to levitate a particle with a focussed Gaussian laser beam can be calculated from the equations reported by Barton *et al.*,[7] allowing the estimation of the mass of the particle. These calculations are complicated by the Bessel beam profile and the requirement in these measurements to introduce the downward air flow. Consequentially we chose to investigate a method that has no such complication. Lorenz–Mie theory is used extensively to interpret the light scattering from spherical particles. The intensity of scattered light at a fixed angle can be interpreted as a function of size parameter. Further, the scattering intensity over a range of angles can be measured and compared to predictions from Mie theory to determine the droplet size.[8] Although scattering of a Bessel beam by a sphere has been considered before,[9] Mie theory is formulated for the illumination of a particle by a plane wave. Thus, a loosely focused HeNe beam was introduced as a source of incident radiation for scattering measurements independent of scattering from the Bessel beam.

Once the droplet is stable in position within the trap (Fig. 2a), the HeNe diffraction pattern can be collected on the CCD camera, as shown in Fig. 2b. The circular collection aperture is defined by a 50 mm diameter lens positioned one focal length (50 mm) from the trap and defines the range of angles over which the phase function is collected. These images are vertically compressed to give the 1-d phase function shown in Fig. 2c. By comparison with Mie scattering simulations of droplets of varying size, the diameter of the trapped droplet can be estimated with an accuracy of ±0.2 μm. The best fit Mie simulation is also shown for comparison with each of the experimental phase plots. In the simulation, the refractive index of the droplet is assumed to be equal to that of the bulk solution. The change in concentration through droplet evaporation will lead to a change in this refractive index and hence an error in the size determined. In an extreme example, a change in radius by a factor of two will lead to an 8-fold change in concentration and a ~5% change in refractive index. A discrepancy in refractive index of this magnitude could result in a size error of ±100 nm in diameter.

An uncertainty of approximately 3° in the geometry of the elastic scattering collection angle introduces a further error in the size of ±0.2 μm. The range of particle sizes that were observed within the Bessel beam and for which we were able to estimate sizes from their phase functions is between 1.8 and 6.8 μm in diameter. All quoted droplet sizes are subject to the accumulation of these errors, conservatively ±300 nm.

On introduction of the aerosol flow, the water partial pressure in the gas phase throughout the cell rapidly assumes a value equal to the vapour pressure of the solution, approximately 3 kPa in our case, yielding a relative humidity (RH) of *ca.* 95%. The experimental cell is not entirely enclosed and after nebulisation has ceased the RH steadily decreases to that of the surrounding environment as laboratory air is drawn in by the air pump. The process is slowed by the presence of dispersed aerosol in the cell and liquid water that has deposited on the cell walls. However, over time, the droplets steadily decrease in size reflecting the decreasing

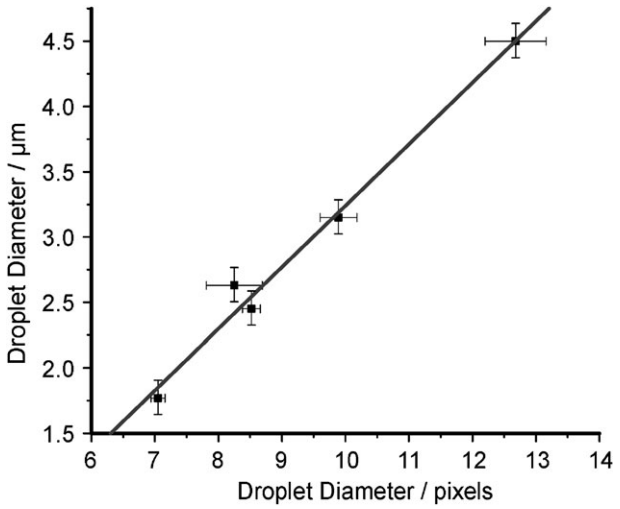

Fig. 3 Calibration plot for bright field image sizing. The droplet diameter is measured using the droplet phase function and the diameter in pixels measured in the bright field image.

RH. Larger particles (around 3 μm diameter and higher) are therefore short lived, shrinking in accordance with the changing RH. The largest particle that was observed in the trap from which a phase function was measured was 6.8 μm in diameter. Since the droplet diameter exceeds the anticipated core size by 1.8 μm, this suggests that the Bessel trap is not limited to droplets smaller than the core. Alternatively, this observation could reflect the uncertainty in the core size estimate and may offer a means for measuring the core diameter. The smallest droplet measurable using the phase function was 1.8 μm in diameter. At this small size, the phase function begins to lose structure as the dimension of the scatterer (the droplet) approaches the wavelength of the laser illumination. To characterise smaller droplets we will need to use shorter wavelength illumination or use a different measurement method.

After calibration using the phase function, the bright field imaging can be used to size trapped droplets. The calibration plot shown in Fig. 3 demonstrates that there is excellent correlation between the dimension of the droplet in the bright field image and the size determined from the phase function analysis.

The bright field method allows us to probe smaller size droplets than the phase function will allow. As a result, it is apparent that particles considerably smaller than 1.8 μm in diameter (or $\sim$7 pixels across in the bright field image) can be found in the Bessel trap. Covering as little as three pixels, these droplets are considerably smaller than 1 μm in diameter. However, at this lower limit the particle size approaches the diffraction limit of *ca.* 0.9 μm imposed by the wavelength of the probe beam (632.8 nm) and the collection optics. Accordingly, the phase function becomes completely featureless. A different approach will be required to precisely characterise these accumulation mode particles. However, to our knowledge this represents the first demonstration that accumulation mode aerosol particles can be captured and manipulated using light over extended periods of time.

IV. Guiding measurements on particles of variable size

With the ability to accurately determine the size of trapped droplets, the nature of the Bessel trap and the guiding of aerosol particles can be explored in more detail. In the following section the particle transport properties of the Bessel beam are studied with respect to particle size, trap position and laser power.

Although the central core is pseudo-non-diffracting, subtle divergence does occur over millimetre length scales and, therefore, the radiation pressure acting on a particle also varies along the direction of beam propagation. Indeed, it is this property that enables particles to find an equilibrium position, trapped in the beam. For a particle in a vertically propagating Bessel beam to remain stable in height, the radiation pressure must be balanced by the sum of the gravitational and drag forces exerted on the particle. Altering the radiation pressure by adjusting the laser power drives the trapped particle to a new equilibrium position offering a means of particle transportation and yielding information on the divergence of the Bessel core.

Fig. 4 shows a series of images of two droplets trapped in the Bessel core as a function of laser power. Both droplets are approximately 1 μm in diameter. From left to right, the *x*-axis of the plot is also representative of time over a total of ten minutes. The figure reflects a stepwise increase in power over time, followed by a stepwise decrease. It is interesting to note that the droplets do not return exactly to the starting position and this can be attributed to a slight reduction in the cell RH over the course of the experiment causing the droplets to shrink in size. It should also be noted that the vertical displacement of the droplets exceeds the imaging area projected onto the CCD, and the position of the camera must be adjusted on a micrometre stage accordingly. The adjustment was done by holding the droplet at the same power and recording the image of the droplet at two different heights of the camera.

The displacement with power is characterised by two regions of approximately linear correlation, from 400 to 800 mW and 800 to 1500 mW. On close examination it is also noticeable that the separation between the two particles increases as a function of laser power, from approximately 5 to 10 μm, shown in Fig. 5. This change in separation may be due to slight imperfections in the beam alignment, leading to slightly different fractional changes in radiation pressure as the laser power is adjusted. However, it is more likely that separation reflects the difference in scattering efficiency for the two particle sizes. If this is the case, it may be possible to use the axial trapping position as a measure of particle size.

The power *versus* displacement measurement was repeated with seven droplets of different size, shown in Fig. 6(a), ranging in size from 1.75 μm in diameter to sub-micron. The same data are presented in Fig. 6(b) after normalising the data to zero displacement at low power. As before the displacement was measured as a function of power in a stepwise increase followed by a stepwise decrease and hence there are two data points for each droplet at each power. It can be seen in Fig. 6(a) that the droplet size has a significant effect on the equilibrium

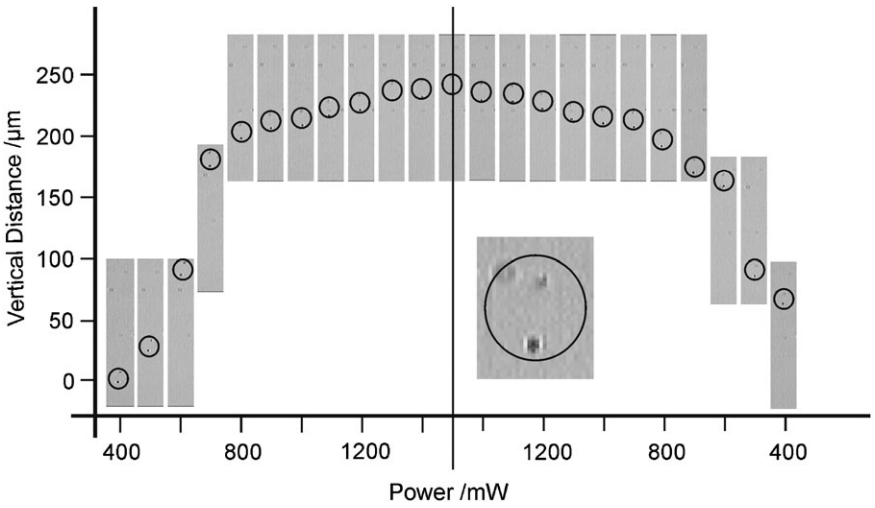

Fig. 4 Bright field images of two droplets trapped in the Bessel beam and plotted on a graph of power *versus* vertical displacement. The droplets are both approximately 1 μm in diameter. The circled region is shown enlarged and inset.

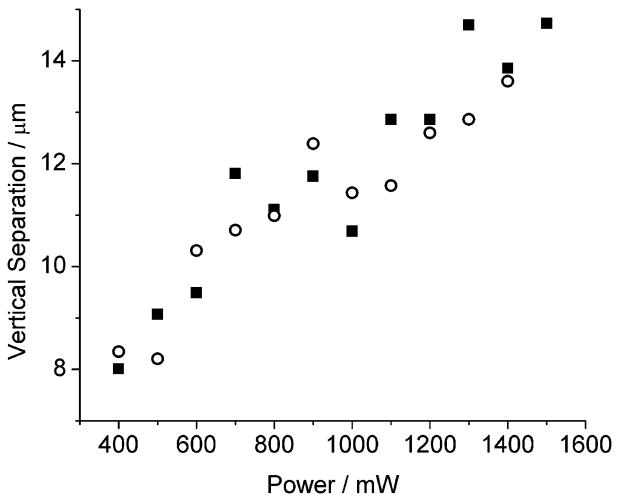

Fig. 5 The vertical separation of two droplets (shown in Fig. 4), as a function of increasing (filled squares) and decreasing (open circles) laser power.

position at any given power, although at this stage we are unable to accurately resolve this relationship due to the uncertainty in droplet size and instabilities in the droplet position over time, seen in Fig. 7 and 8. The guiding distances are approximately the same for all droplets in this size range and show qualitatively the same dependence on laser power with no systematic dependence observed with size within the error of the measurements. The sensitivity of the position to laser power is, on average, 0.25 μm mW^{-1} in this work, compared to 1.25 μm mW^{-1} in our previous work,[3] leading to a maximum guiding distance of 250 μm, considerably less than the 1 mm achieved in our previous work. These differences can be attributed to changes in the experimental set-up. In particular, the downward drag force imposed by the gas flow is not the same in the two experiments. Further, the particle sizes are quite different: in our previous work, less volatile dodecane droplets were studied, and these were estimated to be 7 μm in diameter using bright field microscopy, several times larger than the droplets in the current

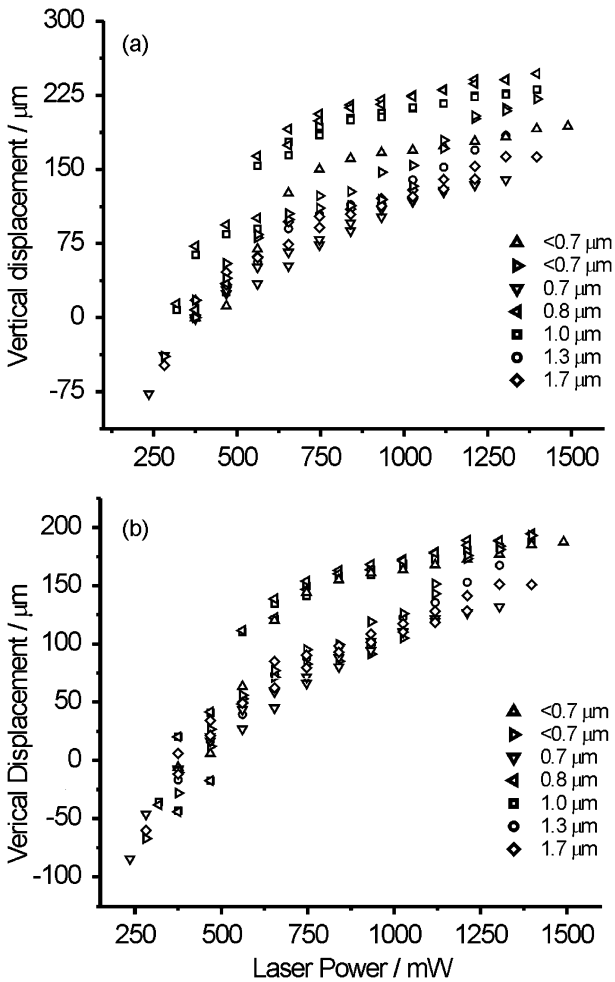

Fig. 6 (a) Vertical displacement of trapped droplets as a function of Bessel beam power. In (b) the displacement is normalised at low power. The minimum power defines the limit at which all of the droplets were stable in the trap. Droplet sizes indicated are diameters.

work. The associated difference in scattering efficiency is likely to account for some of the observed change in guiding distance.

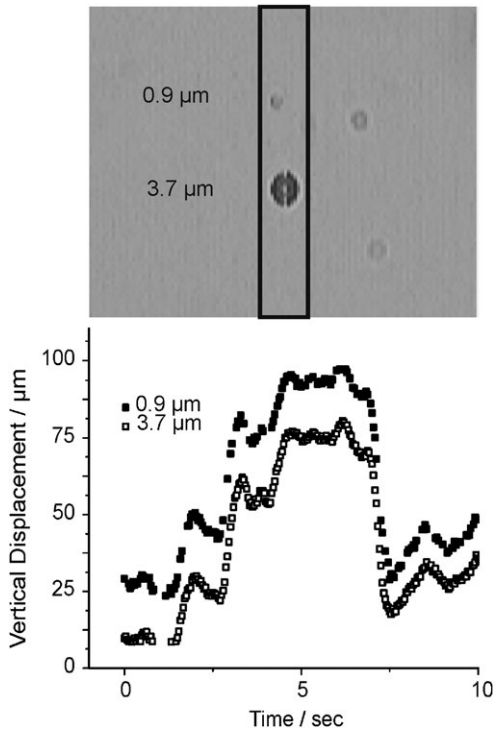

Fig. 7 Axial instability of droplets trapped in the Bessel beam core. Droplet sizes indicated are diameters.

The transverse position of particles in a Bessel beam in the condensed phase has been studied both experimentally and theoretically. Interactions between small particles, the surrounding optical forces, and the dynamic distribution along a periodic optical field show a strong dependence on particle size, refractive index and shape.[10,11] Brownian motion and the influence of tilted and un-tilted Bessel beam geometries influence particle movement through the transverse optical landscape.[12,13]

In the current measurements, the axial equilibrium position of trapped droplets was observed to fluctuate over tens of microns due to instabilities in the experimental conditions on a sub-second timescale. Such motions are shown in Fig. 7 and 8. Depending on their transverse position, the droplet trajectories along the propagation axis can be described by one of two distinct movement patterns. In Fig. 7, droplets are shown stacked within the core along the beam propagation direction. In this case variations in their vertical positions are coherent and any fluctuations occur simultaneously. The second case, as shown in Fig. 8, describes droplets that have distinct transverse positions in the beam. In this case, vertical variations in position are incoherent and less correlated.

If we regard the diameter of the core size to be 5 μm, it is reasonable to propose that pairs of droplets in Fig. 7(a) and (b) are both situated in the core. Their correlated movement is a result of power fluctuations in the beam core and, despite their difference in size, the particles respond to these fluctuations in a similar manner. The amplitude of fluctuations in the vertical position of a trapped particle is typically in the range of 1–30 μm.

Uncorrelated movements of droplets, like those shown in Fig. 8, can be rationalised if the droplets are situated in different radial intensity regions of the beam. In this example the two smaller droplets exhibit coordinated movements, whereas the largest droplet, although preserving some of the coordinated movement, changes in position relative to the other two droplets. This would suggest that there are some power variations in the rings that are not experienced by the particles located in the core and *vice versa*. If we consider that the smaller droplets are in the core, and the largest droplet is in an outer ring of the beam then we can conclude from these observations that there must be some optical instability leading to a redistribution of power between the core and the rings of the Bessel beam. This may be caused by vibrations, fractionally varying the optical alignment or the interaction of dust and aerosol particles with the laser beam upstream of the Bessel beam optics.

V. Conclusions

We have shown an ability to optically trap, manipulate and characterise accumulation and coarse mode aerosol droplets in

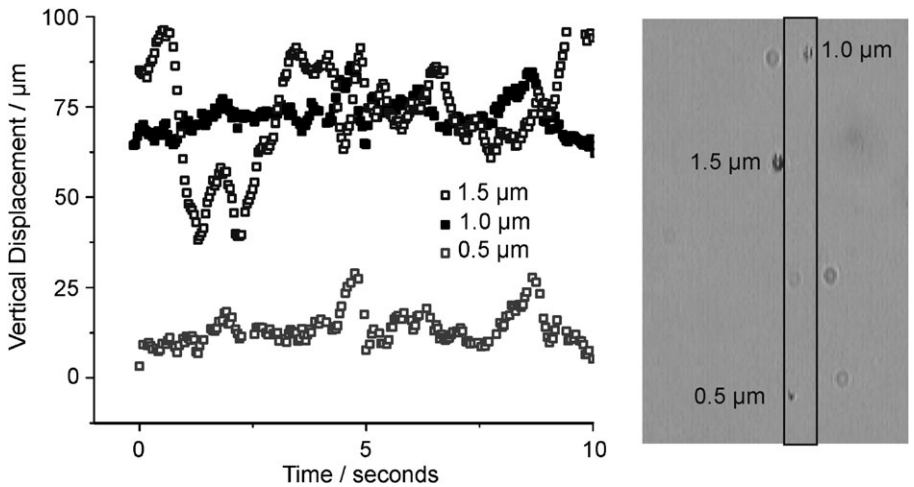

Fig. 8 Axial instability of droplets in the Bessel beam core, marked by the rectangle, and outer rings. Droplet sizes indicated are diameters.

a Bessel beam trap. Droplets with diameters in the range 4.5 μm to sub-micron have been determined using a combination of elastic light scattering and bright field microscopy. We have used characterised particles to probe the transportation properties and potential of a Bessel beam aerosol trap. Further studies are needed to fully rationalise the power *versus* displacement characteristics of the trap in terms of particle scattering efficiency as a function of size. We have found that small instabilities in the optical alignment and variability in the Gaussian power distribution of the source laser can lead to both global fluctuations in the power of the beam and also local variations in the power distribution between the core and the outer rings of the beam.

In our ongoing studies we are implementing shorter wavelength scattering lasers and enhanced bright field microscopy to extend the precision of our sub-micron sizing capabilities. Enhanced resolution of the phase function will enable us to simultaneously characterise refractive index as well as size from this simple measurement.

Optical tweezing is a powerful tool for the study of aerosol particles. The Bessel beam trap presented in this paper represents a valuable addition to the optical tweezers toolkit. Whilst the Bessel beam does not offer the trapping stability or easy compatibility with Raman spectroscopies that single-beam gradient force tweezers can, the Bessel beam has significant advantages in terms of macroscopic transportation, trapping volume and gas phase control. Further and most significantly, the Bessel beam trap extends the lower size limit of aerosol particles that can be studied using optical tweezers into the accumulation mode.

Acknowledgements

The authors gratefully acknowledge support from the EPSRC through support of an Advanced Research Fellowship (JPR), Postdoctoral Research Fellowship (JBW) and in conjunction with the RSC, an Analytical Science Studentship (HM). MDS was also supported by an Analytical Trust RSC/ESPRC Studentship. DM is a Royal Society University Research Fellow. Finally, the authors thank Dr Maria Rodas-Verde for her help at the early stages of this project.

References

1 Climate Change 2007: The Physical Science Basis-Contribution of Working Group to the Fourth Assessment Report of the Intergovernmental Panel on Climate Change (IPCC), 2007.
2 J. Haywood and O. Boucher, *Rev. Geophys.*, 2000, **38**, 513–543.
3 M. D. Summers, J. P. Reid and D. McGloin, *Opt. Express*, 2006, **14**, 6373–6380.
4 Y. Lin, W. Seka, J. H. Eberly, H. Huang and D. L. Brown, *Appl. Opt.*, 1992, **31**, 2708–2713.
5 J. Durnin, J. J. Miceli and J. H. Eberly, *Phys. Rev. Lett.*, 1987, **58**, 1499.
6 A. Ashkin and J. M. Dziedzic, *Science*, 1975, **187**, 1073–1075.
7 J. P. Barton, D. R. Alexander and S. A. Schaub, *J. Appl. Phys.*, 1989, **66**, 4594–4602.
8 G. Mie, *Ann. Phys. (Leipzig)*, 1908, **25**, 377–445.
9 P. L. Marston, *J. Acoust. Soc. Am.*, 2007, **121**, 753–758.
10 G. Milne, K. Dholakia, D. McGloin, K. Volke-Sepulveda and P. Zemánek, *Opt. Express*, 2007, **15**, 13972–13987.
11 T. Cizmar, E. Kollarova, Z. Bouchal and P. Zemanek, *New J. Phys.*, 2006, **8**, 43.
12 S. A. Tatarkova, W. Sibbett and K. Dholakia, *Phys. Rev. Lett.*, 2003, **91**, 038101.
13 L. Paterson, E. Papagiakoumou, G. Milne, V. Garces-Chavez, S. A. Tatarkova, W. Sibbett, F. J. Gunn-Moore, P. E. Bryant, A. C. Riches and K. Dholakia, *Appl. Phys. Lett.*, 2005, **87**, 123901–123903.